INSTITUTE OF PHYSICS PUBLISHING PHYSICS IN MEDICINE AND BIOLOGY

Phys. Med. Biol. **48** (2003) 1491–1504 PII: S0031-9155(03)57708-9

# Time-series estimation of biological factors in optical diffusion tomography

**Simon Prince[1], Ville Kolehmainen[2], Jari P Kaipio[2], Maria Angela Franceschini[3,4], David Boas[4] and Simon R Arridge[5]**

[1] Department of Electrical and Computer Engineering, National University of Singapore, 4 Engineering Drive 3, Singapore 113576
[2] Department of Applied Physics, University of Kuopio, PO Box 1627, 70211 Kuopio, Finland
[3] Bioengineering Center, Department of Electrical and Computer Science, Tufts University, 4 Colby St, Medford, MA 02155, USA
[4] Massachussets General Hospital NMR Centre, Harvard Medical School, Charlestown, MA, USA
[5] Department of Computer Science, University College London, Gower Street, London WC1E 6BT, UK

E-mail: ucacarr@cs.ucl.ac.uk

Received 24 December 2002
Published 20 May 2003
Online at stacks.iop.org/PMB/48/1491

**Abstract**

We apply state space estimation techniques to the time-varying reconstruction problem in optical tomography. We develop a stochastic model for describing the evolution of quasi-sinusoidal medical signals such as the heartbeat, assuming these are represented as a known frequency with randomly varying amplitude and phase. We use the extended Kalman filter in combination with spatial regularization techniques to reconstruct images from highly underdetermined time-series data. This system also naturally segments activity belonging to different biological processes. We present reconstructions of simulated data and of real data recorded from the human motor cortex (Franceschini *et al* 2000 *Optics Express* **6** 49–57). It is argued that the application of these time-series techniques improves both the fidelity and temporal resolution of reconstruction in optical tomography.

M This article features online multimedia enhancements

## 1. Introduction

Optical tomography (OT) refers to the application of low-energy visible or near infrared light to generate images of the optical properties of highly scattering media. Typically, a number of discrete laser sources are positioned at the surface of the medium $\partial\Omega$. Light is transported through the body $\Omega$ and undergoes scattering and absorption. A finite number of detectors then measure the light emerging at various points on the surface $\partial\Omega$. There are

two common measurement schemes (Hebden *et al* 1997): *time domain* systems measure the temporal distribution of photons emerging at the surface of the body in response to impulses of light; *frequency domain* systems measure the modulation amplitude and phase delay of the signal resulting from an intensity modulated source.

Optical tomography aims to use these measurements to reconstruct the scattering and absorption coefficients, $\mu_a$ and $\mu_s$, at each position $\mathbf{r}$ in the medium $\Omega$. When applied in a medical context, these properties can provide information about tissue structure and the distribution of oxygenated and de-oxygenated blood. Proposed applications include mammography (Franceschini *et al* 1997, Nioka *et al* 1997, Tromberg *et al* 1997, Fantini *et al* 1996) and functional brain imaging (Franceschini *et al* 2000, Gratton *et al* 1997, Maki *et al* 1996, 1997, Wenzel *et al* 1996, Kato *et al* 1993, Villringer *et al* 1993, Chance *et al* 1993).

The propagation of light through a highly scattering medium is properly described by the radiative transfer equation (RTE):

$$\left(\frac{1}{c}\frac{\partial}{\partial t} + \hat{\mathbf{s}}\cdot\nabla + \mu_s(\mathbf{r}) + \mu_a(\mathbf{r})\right)\phi(\mathbf{r},\hat{\mathbf{s}},t) = \mu_s(\mathbf{r})\int_{\mathbf{S}^2} p(\hat{\mathbf{s}}'\to\hat{\mathbf{s}})\phi(\mathbf{r},\hat{\mathbf{s}}',t)\,\mathrm{d}\hat{\mathbf{s}}' + q(\mathbf{r},\hat{\mathbf{s}},t) \qquad \mathbf{r}\in\Omega \tag{1}$$

where $\hat{\mathbf{s}}$ is a unit vector in $\mathbf{S}^2$ and $\phi(\mathbf{r},\hat{\mathbf{s}},t)$ is the energy radiance at position $\mathbf{r}$ and time $t$ moving with speed $c$ in direction $\hat{\mathbf{s}}$. The function $p(\hat{\mathbf{s}}'\to\hat{\mathbf{s}})$ gives the probability density (scattering phase function) for scattering from $\hat{\mathbf{s}}'$ to $\hat{\mathbf{s}}$, the function $q$ represents the spatial distribution of photon sources and $\mu_a(\mathbf{r})$ and $\mu_s(\mathbf{r})$ are the absorption and scattering coefficients, respectively.

In order to simplify the forward model, the radiative transfer equation can be approximated by a parabolic diffusion equation (see Arridge (1999) and Heino and Somersalo (2002) for details). In this simplified model, photon transport is described by the relation

$$-\nabla\cdot\kappa(\mathbf{r})\nabla\Phi(\mathbf{r},t) + \left(\mu_a(\mathbf{r}) + \frac{1}{c}\frac{\partial}{\partial t}\right)\Phi(\mathbf{r},t) = q_0(\mathbf{r},t) \tag{2}$$

where $\Phi(\mathbf{r},t) = \int_{\mathbf{S}^2}\phi(\mathbf{r},\hat{\mathbf{s}},t)\mathrm{d}\hat{\mathbf{s}}$ is the photon density, $\kappa = (3(\mu_a + (1-g)\mu_s))^{-1}$ is the diffusion coefficient, with $g$ the average cosine of the scattering phase function $p(\hat{\mathbf{s}}'\to\hat{\mathbf{s}})$, assumed directionally independent, and the function $q_0$ describes an isotropic source component within the medium $\Omega$. It is only possible to derive analytic expressions for the solution of the diffusion equation in special cases such as for a point source in an infinite homogeneous medium. More generally, numerical solutions based on finite differences or finite elements are applied. For a detailed exposition of the use of finite element methods in optical tomography, see Arridge *et al* (1993), Schweiger *et al* (1993, 1995) and Arridge (1999).

The reconstruction of absorption and scattering coefficients based on OT data is a nonlinear ill-posed inverse problem. Most of the current approaches to tackle this ill-posed problem can be classified crudely into three classes that are backprojection methods (Walker *et al* 1997, Colak *et al* 1997), linear (perturbation) methods, see, e.g., Gaudette *et al* (2000), Chang *et al* (1996), and the regularized output least-squares methods, see, e.g., Arridge (1999), Ye *et al* (1999) and Paulsen and Jiang (1996). A common feature to all these methods is that they are static, i.e. they assume that the absorption and scattering coefficients do not exhibit changes during the time that is needed to measure a complete set of data for one traditional image frame.

Current approaches to the dynamic OT problem attempt to reconstruct time-varying absorption and scattering coefficients on an independent frame by frame basis from the sequence of measurements using static reconstruction methods, see, e.g., Bluestone *et al* (2001) and Barbour *et al* (1999). These methods have two intrinsic weaknesses. Firstly, with these

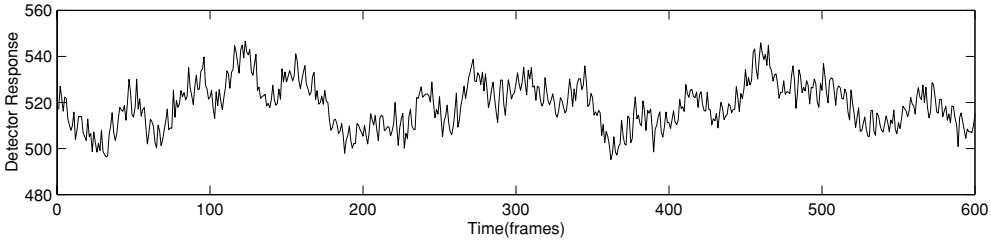


**Figure 1.** Sample of continuous wave (CW) amplitude data from one source–detector pair in the experiment of Franceschini *et al* (2000). The signal has a strong deterministic component. In fact, oscillatory components at three different scales can be identified, which probably correspond to arterial pulsation, breathing and the experimental manipulation which alternated between two conditions.

methods one may lose most of the temporal information when the rate of change in the absorption and scattering coefficient is fast compared to the time that is needed to collect a complete dataset for one traditional image frame. Secondly, since we are observing biological processes, it seems inappropriate to assume (implicitly) that the optical properties of the tissue should be completely unrelated at nearby time instants. To illustrate this point, we reproduce measurements of the motor cortex from Franceschini *et al* (2000) in figure 1. The plot reveals that the measurements, and by extension, the optical properties of the tissue, have a deterministic component. In fact, three oscillating components can be seen which correspond to the heartbeat, breathing and experimental stimulus, respectively. Taken together, these arguments can be taken as meaning that there may be no consistent static solution for data measured at different times.

This paper attempts to render the reconstruction of time-varying absorption and scattering coefficients more tractable by making use of time-series information in the measurement stream. The basic method is to construct a stochastic model for the random process underlying the measurement sequence. We utilize this model to generate a Bayesian prior for the dynamic reconstruction of the absorption and scattering coefficients in turn, using a method based on Kalman filtering techniques. Similar state space estimation approaches have been previously applied to electrical impedence tomography (EIT) in Kaipio *et al* (1999), Kaipio and Somersalo (1999), Vauhkonen *et al* (1999, 2001) and Seppänen *et al* (2001a, 2001b) and to optical tomography in Kolehmainen *et al* (2003) but only with simulated data. In addition to demonstrating the application of state space methods to optical tomography, the main contribution of this paper is to develop a suitable state update model for describing oscillating biological signals and to apply the method to real data from the study of Franceschini *et al* (2000).

In the first part of the paper we describe the standard approach to the static reconstruction based on the traditional image frame. We then introduce a novel method to the dynamic reconstruction based on the state space estimation. We propose a stochastic model for describing biological activity and present a simulation in which we reconstruct and segment a time series of images. Finally, we demonstrate the practical application of this scheme by reconstructing data from the experimental work of Franceschini *et al* (2000).

## 2. Static reconstruction approach

The static reconstruction approach can be stated for each frame as follows. Given a known array of source inputs $\{q\}$ and a known set of measurements $\{y\}$ at detector positions $\{d\}$ on

the boundary, $\partial\Omega$, we must reconstruct the absorption and scattering properties $\mu_a(\mathbf{r})$, $\mu_s(\mathbf{r})$ of the medium $\Omega$. Although there is generally no closed form solution to this problem, the tractability of the forward problem (the diffusion equation) admits an obvious numerical approach. For notational simplicity, we concatenate the optical properties, $\mu_a(\mathbf{r})$ and $\mu_s(\mathbf{r})$, into a single vector, $\mathbf{x}$, and the measurements into a vector $\mathbf{y}$. If the forward mapping is expressed as $\mathbf{y} = f(\mathbf{x})$, then one can consider the reconstruction problem as a minimization of the total-squared error

$$E(\mathbf{x}) = \frac{1}{2}\|\mathbf{y} - f(\mathbf{x})\|^2_{\mathsf{R}^{-1}} = \frac{1}{2}\sum_{q=1}^{Q}\sum_{d=1}^{D}\left(\frac{y_{q,d} - f_{q,d}(\mathbf{x})}{\sigma_{q,d}}\right)^2 \tag{3}$$

where $q$ is the source number, $d$ is the detector number and $\mathsf{R}$ is the covariance matrix associated with the measurement noise, which is here taken to be diagonal with entries $\sigma^2_{q,d}$ specifying the variance associated with this measurement. Because the problem (3) is ill posed, Tikhonov regularization techniques are used to stabilize the problem by imposing (spatial) prior knowledge about the optical properties of the medium (Arridge 1999, Ye *et al* 1999, Paulsen and Jiang 1996). In most cases the modified problem is written in the form

$$E_{\text{Tikh.}}(\mathbf{x}) = E(\mathbf{x}) + \alpha\|\mathsf{L}\mathbf{x}\|^2 \tag{4}$$

where $\mathsf{L}$ is the regularization matrix (e.g., a discrete approximation to a differential operator) and $\alpha > 0$ is the regularization parameter.

A typical numerical approach to minimize the error functional (4) is to use iterative optimization methods such as the Gauss–Newton method:

$$\mathbf{x}_{n+1} = \mathbf{x}_n + (\mathsf{J}(\mathbf{x}_n)^{\mathrm{T}}\mathsf{R}^{-1}\mathsf{J}(\mathbf{x}_n) + \alpha\mathsf{L}^{\mathrm{T}}\mathsf{L})^{-1}(\mathsf{J}(\mathbf{x}_n)^{\mathrm{T}}\mathsf{R}^{-1}[\mathbf{y} - f(\mathbf{x}_n)] - \alpha\mathsf{L}^{\mathrm{T}}\mathsf{L}\mathbf{x}_n) \tag{5}$$

where $\mathsf{J}(\mathbf{x}_n) = f'(\mathbf{x}_n)$ is the Jacobian containing derivatives of the terms $y_{q,d}$ with respect to components of $\mathbf{x}$, evaluated at $\mathbf{x}_n$.

## 3. State space reconstruction approach

In the state space approach to dynamic image reconstruction, we consider the optical properties of the medium, $\mathbf{x}$, to be a discrete time stochastic process governed by a stochastic difference equation. We denote this as the state update model and will assume linearity so that it takes the form

$$\mathbf{x}_k = \mathsf{K}\mathbf{x}_{k-1} + \mathbf{n}_k \tag{6}$$

where the state transition matrix $\mathsf{K}$ gives the deterministic part of the state update model, $\mathbf{n}_k$ is a Gaussian random vector and the subindice $k$ denotes the (integer) time steps. Nonlinear state update models are also possible but will not be considered in this paper. As before, we assume that the measurements are derived from the state using the forward model with Gaussian additive noise:

$$\mathbf{y}_k = \mathbf{f}_k(\mathbf{x}_k) + \mathbf{m}_k \tag{7}$$

where the observation vector $\mathbf{y}_k$ contains measurements that are acquired at time instant $k$ and $\mathbf{f}_k(\cdot)$ is the part of the forward model that corresponds to $\mathbf{y}_k$, which is acquired sufficiently quickly so that it can be assumed that the state vector $\mathbf{x}_k$ was constant during the acquisition. This last point is important in the application of dynamic reconstruction methods, and can encompass several scenarios. For example, in one configuration $\mathbf{y}_k$ may consist of a single observation between one source and one detector, or if all detector channels are measured in parallel, it may contain the responses of all the detectors to a given source; at the other extreme,

it would be a fast measurement system (or slowly varying state) in which all excitations were assumed simultaneous. The dynamic reconstruction framework is flexible enough to accommodate all these conditions, but in this paper we concern ourselves with the intermediate case in which each source is excited in serial and the measurements taken in parallel.

The dynamic reconstruction technique splits the update of state $\hat{\mathbf{x}}_{k-1} \rightarrow \hat{\mathbf{x}}_k$ at time $k$ into an optimal estimate based on (i) the prediction of the state update model, $\hat{\mathbf{x}}_k^{(-)}$ from the previous state $\hat{\mathbf{x}}_{k-1}$ and (ii) the noisy measurement, $\mathbf{y}_k$,

$$\hat{\mathbf{x}}_{k-1} \rightarrow \hat{\mathbf{x}}_k^{(-)} \rightarrow \hat{\mathbf{x}}_k.$$

It is easy to see how this can help with the ill-conditioned inverse problem: when the measurement, $\mathbf{y}_k$, does not adequately constrain the state, $\mathbf{x}_k$, the temporal priors (the predictions) that are based on the time-series model help us to ensure that a sensible solution is adopted. For linear state update and measurement models, with Gaussian statistics, the well-known Kalman recursions provide a closed form solution to this problem. Unfortunately, the measurement (forward) model (7) is nonlinear. In nonlinear cases, suboptimal estimates can be obtained by writing linear approximations for the nonlinear measurement and/or state update models, and then applying the Kalman recursions. This approach is known as the extended Kalman filter, in which we linearize the forward model (7) about the predicted state estimate. We retain a linear state update model. With these choices, the full update equations for the extended Kalman filter are given by

*State prediction*:

$$\hat{\mathbf{x}}_k^{(-)} = \mathsf{K}\hat{\mathbf{x}}_{k-1} \tag{8}$$

*Variance prediction:*

$$\mathsf{C}_k^{(-)} = \mathsf{K}\mathsf{C}_{k-1}\mathsf{K}^{\mathrm{T}} + \mathsf{Q}_k \tag{9}$$

*Kalman gain:*

$$\mathsf{G}_k = \mathsf{C}_k^{(-)}\mathsf{J}_k^{\mathrm{T}}\left(\mathsf{J}_k\mathsf{C}_k^{(-)}\mathsf{J}_k^{\mathrm{T}} + \mathsf{R}_k\right)^{-1} \tag{10}$$

*State update:*

$$\hat{\mathbf{x}}_k = \hat{\mathbf{x}}_k^{(-)} + \mathsf{G}_k\left(\mathbf{y}_k - \mathbf{f}_k\left(\hat{\mathbf{x}}_k^{(-)}\right)\right) \tag{11}$$

*Variance update:*

$$\mathsf{C}_k = (\mathsf{I} - \mathsf{G}_k\mathsf{J}_k)\mathsf{C}_k^{(-)} \tag{12}$$

where $\mathsf{C}$ is the covariance matrix describing the uncertainty of the state, $\mathsf{Q}$ is the covariance matrix associated with the state update noise vector $\mathbf{n}_k$, $\mathsf{R}$ is the covariance of the observation errors $\mathbf{m}_k$ and $\mathsf{J}_k$ is the Jacobian of $\mathbf{f}_k\left(\hat{\mathbf{x}}_k^{(-)}\right)$, evaluated at $\hat{\mathbf{x}}_k^{(-)}$. $\mathsf{G}$ is a pseudo-inverse that incorporates the model and the new measurements and is termed the Kalman gain. In this notation the superscript $(-)$ refers to the intermediate state and covariance predictions provided by the state update model, which are then modified by the measured data to produce the next state value. The system (8)–(12) is initialized with a first state estimate $\hat{\mathbf{x}}_0$, and an initial covariance $\mathsf{C}_0$, which is usually taken to be a large multiple of the identity matrix, reflecting the fact that our knowledge of the parameters prior to any estimates is weak. The effect of this 'large' initialization tails off after a few Kalman recursions. A readable introduction to the Kalman filter and its variants can be found in Anderson and Moore (1979).

This recursive formulation means that only data received up to the current time instant contribute to the final answer. In order to incorporate data from future points in the sequence, we apply the fixed interval Kalman smoother. The forward Kalman filter ((8)–(12)) performs a complete forward sweep of the dataset. Subsequently, a backward sweep is carried out which

adjusts each estimate to incorporate the information received after the original estimate was made. Consider a fixed-length interval consisting of $N$ time instants. It was shown by Rauch *et al* (1963) that the adjusted estimates, $\hat{\mathbf{x}}_{k|N}$, may be determined by

$$\hat{\mathbf{x}}_{k-1|N} = \hat{\mathbf{x}}_{k-1} + \mathsf{A}_{k-1}\left[\hat{\mathbf{x}}_{k|N} - \hat{\mathbf{x}}_k^{(-)}\right] \tag{13}$$

where the smoothing gain, $\mathsf{A}_k$, is given by

$$\mathsf{A}_{k-1} = \mathsf{C}_{k-1}\mathsf{K}_{k-1}^{\mathrm{T}}\mathsf{C}_k^{(-)-1}. \tag{14}$$

The backward recursions do not require the raw data, since these are incorporated in the estimates from the forward sweep. The reverse sweep is initialized by letting $\hat{\mathbf{x}}_{N|N} = \hat{\mathbf{x}}_N$.

As before, we can also iterate the system to give improved results. The extended Kalman filter and smoother are run through the entire dataset. On the following pass through the data, the Jacobian is calculated around the previous smoothed estimate. The state estimate equation is modified to

$$\hat{\mathbf{x}}_k = \hat{\mathbf{x}}_k^{(-)} + \mathsf{G}_k\left[\mathbf{y}_k - \mathbf{f}_k(\mathbf{x}_k^*) - \mathsf{J}_{x_k^*}\left[\mathbf{x}_k^{(-)} - \mathbf{x}_k^*\right]\right] \tag{15}$$

where the linearization point $\mathbf{x}_k^*$ is the estimate of the state at time $k$ from the previous smoothing run. In principle, the position at which the Jacobian is calculated should become more optimal with each pass through the data, and hence the linear approximation should improve.

Just as in the static case, it is also possible to apply spatial priors to help make the reconstruction well posed (Kaipio and Somersalo 1999). Recall that the linearized measurement equation can be expressed as

$$\mathbf{y}_k \approx \mathbf{f}_k(\hat{\mathbf{x}}_k) + \mathsf{J}_k[\mathbf{x}_k - \mathbf{x}_k^*] + \mathbf{m}_k. \tag{16}$$

Rearranging and combining with a linear penalty term on the solution, we form an augmented measurement model

$$\begin{bmatrix} y_k - \mathbf{f}_k(\mathbf{x}_k^*) + \mathsf{J}_k\mathbf{x}_k^* \\ 0 \end{bmatrix} = \begin{bmatrix} \mathsf{J}_k\mathbf{x}_k \\ \alpha\mathsf{L}\mathbf{x}_k \end{bmatrix} + \begin{bmatrix} \mathbf{m}_k \\ \mathbf{v} \end{bmatrix} \tag{17}$$

where $\mathbf{x}_k^*$ is the linearization point, $\mathsf{L}$ is the regularization operator and $\mathbf{v}$ is a Gaussian random vector. The regularization parameter $\alpha$ and the width of the covariance of $\mathbf{v}$ control the degree to which the solution is attracted to the null space of the regularization operator in the Kalman recursions.

In principle, an alternative to the local state prediction mechanism inherent in the Kalman filtering technique would be to treat the entire dataset for a short time series simultaneously and construct a solution using the Tikhonov regularization with spatial-temporal covariance, assuming a fixed linearization point throughout the time series (i.e. the linearization point at time $t + 1$ does not depend on the solution at time $t$). The treatment of the problem in this paper can be interpreted as a specification of a spatial-temporal covariance under the first-order Markov model for time evolution. Explicit construction of spatio-temporal covariances for other than first-order Markov processes is not straightforward to approach. However, there are also other recent treatises of nonstationary inverse problems that are based on deterministic interpretation of the variables (Schmitt and Louis 2002, Schmitt *et al* 2002). These methods have the drawback that they lack systematic parameter error estimates. The computational feasibility of this approach to nonlinear problems has yet to be studied.

## 4. Modelling biological signals

Many biological signals, including the data presented in figure 1, contain oscillatory components. We aim to utilize this knowledge to build a plausible state update model.

Following figure 1, we consider the optical properties at each point in the image space to be the sum of three quasi-sinusoidal signals,

$$\mu_a(r_i) = \sum_{j=1}^{3} a_{i,j} \cos(2\pi\omega_j t) + b_{i,j} \sin(2\pi\omega_j t) \tag{18}$$

where the coefficient $a_{i,j}$ is the amplitude of the co-sinusoidal oscillatory component of frequency $\omega_j$ at position $i$, and $b_{i,j}$ is the amplitude of the sinusoidal component. Here we are defining quasi-sinusoidal to mean a signal with a known frequency but where amplitude and phase are random variables. We now consider the state vector, $\mathbf{x}$, to consist of all the coefficients $\{a_{i,j}, b_{i,j}\}$ such that

$$\mathbf{x} = \begin{bmatrix} \vdots \\ a_{i,1} \\ b_{i,1} \\ a_{i,2} \\ b_{i,2} \\ a_{i,3} \\ b_{i,3} \\ \vdots \end{bmatrix}. \tag{19}$$

The state update model is modelled as a Wiener process or random walk

$$\mathbf{x}_k = \mathbf{x}_{k-1} + \mathbf{n}_k \tag{20}$$

where $\mathbf{n}_k$ is a noise vector. This simple choice of state update means that $\mathsf{K} = \mathsf{I}$ and each random variable is modelled as an identical independent Brownian random walk. Other choices are certainly possible, but this choice represents the simplest one in the absence of explicit prior knowledge of the state variation. Since the coefficients $a_{j,k}$, $b_{j,k}$ vary smoothly, the overall effect at each frequency is of a narrow band signal, in which the amplitude and phase change slowly over time. The speed of this change (and hence the bandwidth) depends on the magnitude of the random components, $\mathbf{n}_k$. We now aim to reconstruct these six coefficients at each position in the medium. We incorporate the time-varying sum in equation (18) into the forward model and the Jacobian accordingly. The sum of the frequency components can be obtained by the matrix operations,

$$\mathsf{Z}_k = (\cos(2\pi\omega_1 t_k), \sin(2\pi\omega_1 t_k), \cos(2\pi\omega_2 t_k), \sin(2\pi\omega_2 t_k), \cos(2\pi\omega_3 t_k), \sin(2\pi\omega_3 t_k)) \otimes \mathsf{I} \tag{21}$$

where $\otimes$ represents the Kronecker product, and $\mathsf{I}$ is an $M \times M$ identity matrix, where $M$ is the total number of voxels in the reconstruction. Thus we have

$$\mu = \mathsf{Z}_k \mathbf{x}_k. \tag{22}$$

The forward model becomes $\tilde{\mathbf{f}}_k = \mathbf{f}_k(\mathsf{Z}_k \mathbf{x}_k)$ and the Jacobian $\tilde{\mathsf{J}}_k = \mathsf{J}_k \mathsf{Z}_k$.

We now present a simulated example of this type of reconstruction.

## 5. Simulation details

We generated a test dataset which consisted of a sequence of two-dimensional $12 \times 12$ pixel images (see figure 2(a)). For each time instant, the distribution of the absorption coefficient, $\mu_a(\mathbf{r})$, consisted of the linear sum of three overlapping Gaussian components, each of which

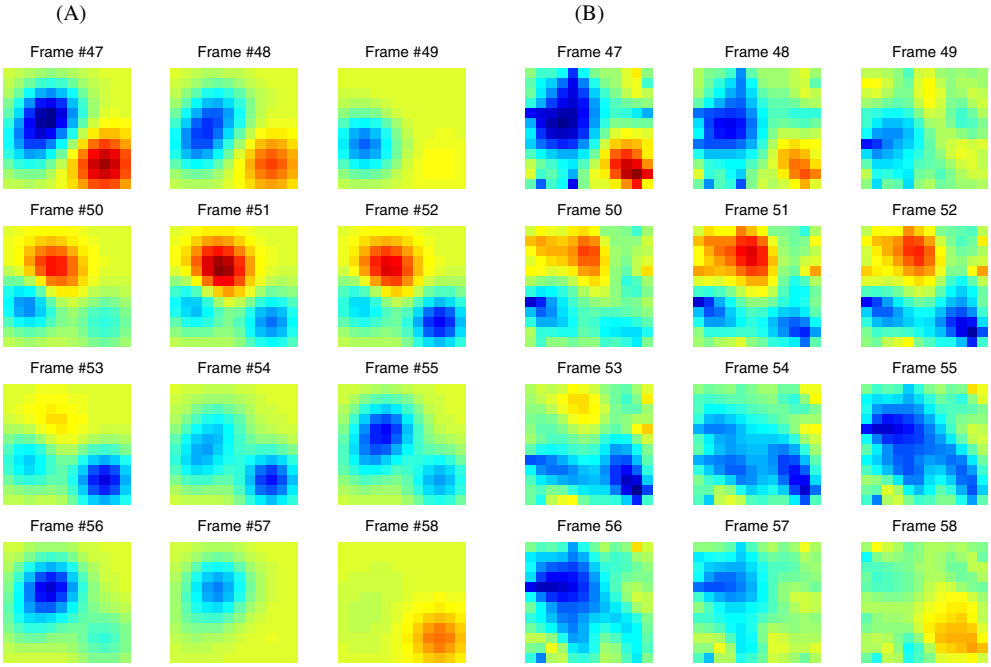


**Figure 2.** (A) and (B) The true absorption distributions and their state estimate reconstructions from the simulated sequence at 12 time instants, respectively. The sequence consists of three overlapping blobs. Each has a narrowband time course with different mean frequency. The main features of the original sequence are captured by the reconstructions.

M An MPEG movie of this figure is available from stacks.iop.org/PMB/48/1491.

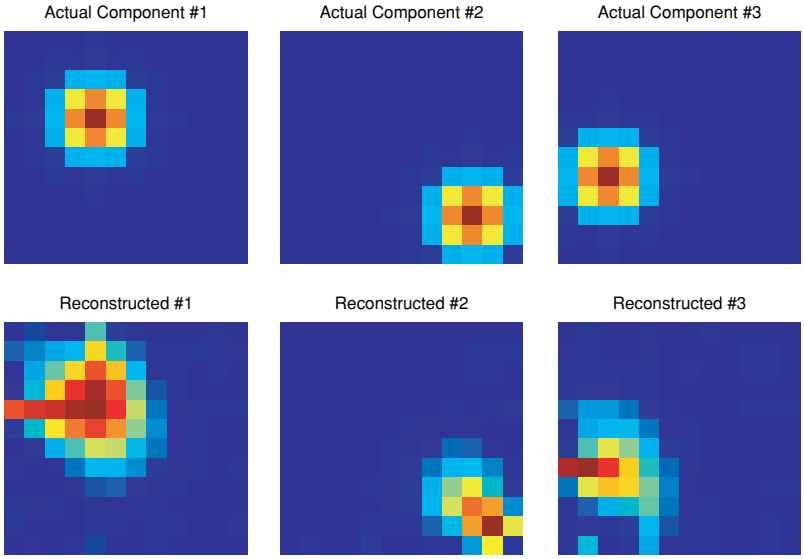


**Figure 3.** The state vector contains the amplitudes of the separate oscillating components. Hence, it is possible to visualize a map of the activity of each. The actual square deviation from the mean value is shown in the top row, and the reconstructed maps are shown below. The reconstruction successfully segments the image.

was quasi-sinusoidal in time, with differing mean frequencies of 0.1111 Hz, 0.0654 Hz and 0.0300 Hz, respectively. The distribution of scattering coefficients $\mu_s(\mathbf{r})$ is assumed constant and known. We simulate eight detectors and eight sources which are alternately and equally spaced around the exterior boundary $\partial\Omega$. Each source fires alternately and yields simultaneously eight measurements of continuous wave (CW) intensity from the detectors, leading to a measurement vector $\mathbf{y}_k \in \mathbb{R}^{8\times 1}$ at each time instant. Thus, the time that is needed to measure a complete dataset $\mathbf{y} \in \mathbb{R}^{64\times 1}$ for one traditional (static) image frame consists of eight time instants. The forward model is implemented using a simple finite difference approximation to the diffusion equation, with Dirichlet conditions assuming the photon density is always zero on the boundary. The Dirichlet boundary condition is not the most appropriate one for photon propagation in tissue, a more correct model being the Robin boundary condition (known as the *partial current* boundary condition in optics, Schweiger *et al* 1995), but since we are using relative measurements normalized to a baseline, the differences are largely cancelled out.

The detector measurements are taken as the photon density $\Phi$ at the exterior boundary next to the detector. Independent noise samples drawn from a normal distribution were added to each measurement where the standard deviation of the noise was equal to 1% of the mean signal level from the detector over the whole sequence.

The image sequence was reconstructed using the state space estimation method described above. The Jacobian matrix J was calculated using the adjoint method (Arridge 1995, 1999). Each row of the Jacobian, which, loosely speaking, relates infinitesimal changes in $\mu_a$ to the infinitesimal changes in the measurement from source $q$ and detector $d$, consists of a photon measurement density function (PMDF), $\rho$, (Arridge and Schweiger 1995) and is given by the expression

$$\mathsf{J}_{q,d} = \rho(\mathbf{r}, \mathbf{r}_q, \mathbf{r}_d) = -G^+(\mathbf{r}, \mathbf{r}_d)G(\mathbf{r}, \mathbf{r}_q) \tag{23}$$

where $G(\mathbf{r}, \mathbf{r}_q)$ is the Green's function propagating from the position of source $\mathbf{r}_q$ and $G^+(\mathbf{r}, \mathbf{r}_d)$ is the adjoint Green's function propagating from the position of detector $\mathbf{r}_d$. In simple terms, the PMDF is the pointwise product of the solutions to the diffusion equation with a unit source at the position of $q$ with that of the solution with a unit source at the position of $d$. In the discrete framework of a finite subspace method such as that used here, the function $\rho$ is projected into the basis representing the coefficients $a_{i,j}, b_{i,j}$. The Jacobian relating the detector measurements to the oscillatory parameters $a_{i,j}$ and $b_{i,j}$ is calculated as described in the previous section.

Figure 2(a) shows the simulated absorption distribution at 12 consecutive time instants. Example reconstructions of this simulated dataset after two passes of the Kalman filter and smoother are shown in figure 2(b). These were calculated by summing the three recovered frequency components, as described in equation (18). The recovered images represent well the structure of the original images.

Note that the state estimate is generated each time a source is fired. We have only eight noisy measurements with which to reconstruct (144 $\times$ 6) coefficients (144 pixels). For a given time instant, the measurements may contain information only from a part of the image space, but the reconstruction remains stable because the state update model predicts the results elsewhere. As described above, we also simultaneously apply spatial regularization to help make the problem well posed, using a discrete approximation to the two-dimensional Laplacian for the regularization operator. Furthermore, the state space estimation approach has obvious advantages. Firstly, the temporal resolution of the state space reconstruction is eight times higher than the case if a series of static reconstructions was made from each complete set of source–detector responses. Secondly, each observation is integrated into the reconstruction

at the exact time it is received. For example, in the case of Franceschini *et al* (2000), the acquisition of a traditional frame might be spread out over a 160 ms period. Thirdly, the Jacobian, J, is reduced in size, increasing reconstruction speed, although this is not the case if we simultaneously apply spatial regularization as in (15).

One advantage of estimating the coefficients of the individual narrow band components is that it is easy to examine the spatial distribution of each part. Figure 3 shows the mean energy at each frequency, as calculated from the sum of the squares of the coefficients over the whole time series. The reconstruction has successfully segmented the structural components of the original images.

## 6. Reconstructing experimental data

Franceschini *et al* (2000) presented a method for non-invasive imaging of a $9 \times 4$ cm$^2$ area of the brain in which a complete set of measurements is collected every 160 ms. This is faster than twice the heart rate and so it is possible to image arterial pulsation. The apparatus consisted of 16 intensity modulated laser diodes and two heterodyned photo-multiplier tube detectors. We restrict our analysis to the continuous wave component of the eight sources which carried light at 758 nm, giving a total of 16 source–detector pairs. However, of these, six are sufficiently distant from one another that the measured signal is negligible, leaving a total of only ten separate measurements, collected over a period of 160 ms. Data were collected from the human motor cortex during two alternating conditions, in which the subject performed a hand tapping task, or rested respectively.

We reconstructed these data using the state space estimation techniques described above. An exact model predicting measurement values within the tolerance of experimental noise requires a highly sophisticated 3D numerical scheme, incorporating techniques for handling non-scattering voids, anisotropies and boundary coupling effects. However, if we consider only *relative differences* in data from a baseline measurement we can employ a cruder model. Nevertheless, it is important to consider both 3D effects, and also the effect of layers of skin and bone in the head which quite dramatically change the spatial form of the PMDF functions (Arridge and Schweiger 1995).

We construct a finite difference grid of size $21 \times 11 \times 4$ (width $\times$ height $\times$ depth) within which to reconstruct the data. Each element was $0.5\,\text{cm} \times 0.5\,\text{cm} \times 0.5\,\text{cm}$ for compatibility with the back-projected reconstructions presented in the original paper. We model the four layers as skin ($\mu_a = 0.022\,\text{mm}^{-1}$, $\mu_s = 1.000\,\text{mm}^{-1}$), bone ($\mu_a = 0.025\,\text{mm}^{-1}$, $\mu_s = 1.000\,\text{mm}^{-1}$), grey matter ($\mu_a = 0.020\,\text{mm}^{-1}$, $\mu_s = 0.550\,\text{mm}^{-1}$) and white matter ($\mu_a = 0.01\,\text{mm}^{-1}$, $\mu_s = 2.000\,\text{mm}^{-1}$), where these parameters define the diffusion constant $\kappa$ for each layer. The structure of the model together with the placement of the sources and detectors in the original experiment is depicted in figure 4. Since heart rate and respiration were measured in the original experiment, we calculate the model frequencies in (18) from the Fourier transform of these data. The frequency with which the experimental independent variable (i.e. hand tapping) changed is similarly known *a priori*.

The reconstruction is highly underdetermined—at each time instant $k$, we aim to reconstruct $924 \times 6$ parameters (924 voxels, 6 amplitude coefficients) from only two independent measurements (i.e. $\mathbf{y}_k \in \mathbb{R}^{2\times 1}$), one of which is often impossibly noisy.

In order to make the reconstruction tractable, we assume that only the absorption coefficients in the third layer (grey matter) change as a function of time. This reduces the number of parameters to be estimated to $231 \times 6$ and the number of voxels to only 231. In practice, this is achieved by using the full three-dimensional forward model, but only taking the rows of the Jacobian that correspond to parameters from the layer representing the grey matter.

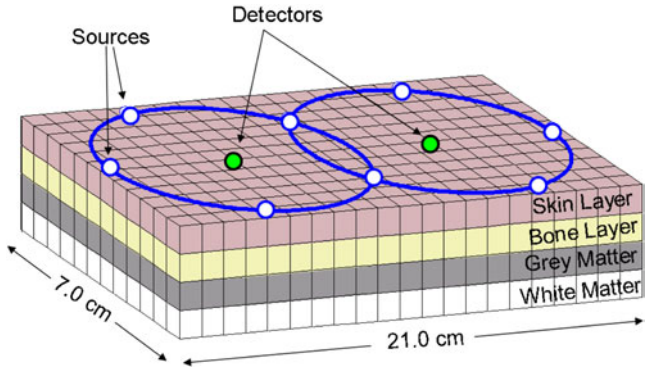


**Figure 4.** Experimental arrangement and grid model. Eight detectors measured light from two sources giving a total of 16 measurements per frame. We divide the volume under the measurement positions into a regular grid of $21 \times 12 \times 4$ voxels. The four layers represent skin, bone, grey and white matter, respectively. We treat all layers apart from the grey matter as having constant absorption properties.

There are two problems associated with reconstruction from real data, which were not encountered in the simulations. Firstly, the level of noise in each source–detector pair may differ and therefore we must estimate the measurement covariance matrix $\mathsf{R}$. Ideally, this should be established experimentally by imaging a constant medium. However, for our post hoc reconstruction we must estimate it from the data itself. We assume that the noise for each source–detector pair is independent of all the others, and proportional to the total variation within that measurement channel. Hence, the measurement distance metric, $\mathsf{R}$, is defined as a diagonal matrix with the channel covariance values on the diagonal.

Secondly, the forward model does not provide estimates of the detector responses which are equivalent to the real equipment. One reason for this is the unknown attenuation which occurs at the coupling between the tissue and the sources and detectors. We must employ a baseline level $\mathbf{y}_{\text{base}}^{\text{meas}}$ that is compatible with the measurements defined by the real detectors. We normalize the measurements to have a mean value of unity and we can similarly define a normalizing vector $\mathbf{y}_{\text{base}}^{\text{calc}} = f(\mathbf{x}_{\text{base}})$, where $y_{\text{base},q,d}^{\text{calc}}$ is equal to the predicted measurement at detector $d$, with a source $q$ of unity amplitude and a homogeneous medium. Effectively, we have now formed a modified measurement model at the core of our state space formulation

$$\tilde{f}(\mathbf{x}) = \frac{\mathbf{y}_{\text{base}}^{\text{meas}}}{f(\mathbf{x}_{\text{base}})} f(\mathbf{x}) \tag{24}$$

where the vector multiplications and divisions are taken to be pointwise. This model has the property of agreeing completely with the data at the point taken as the baseline. When linearization is carried out, and including the estimate of the standard deviation of noise, we get

$$\frac{\mathbf{y}_k^{\text{meas}} - \mathbf{y}_{\text{base}}^{\text{meas}}}{\sigma \mathbf{y}_{\text{base}}^{\text{meas}}} = \frac{\mathsf{J}}{\sigma f(\mathbf{x}_{\text{base}})} [\mathbf{x} - \mathbf{x}_{\text{base}}] \tag{25}$$

where $\sigma$ has entries $\sigma^{(q,d)}$ equal to the estimated standard deviation of the noise on the signal from source $q$, as measured by detector $d$, and the matrix vector division is taken to mean division of the rows of the Jacobian by each term in the vector.

Example reconstruction results after a single forward and backward pass through the time series are shown in figure 5 for a series of frames from the sequence. Note how much structural change is there between consecutive time instants despite the small number of measurements

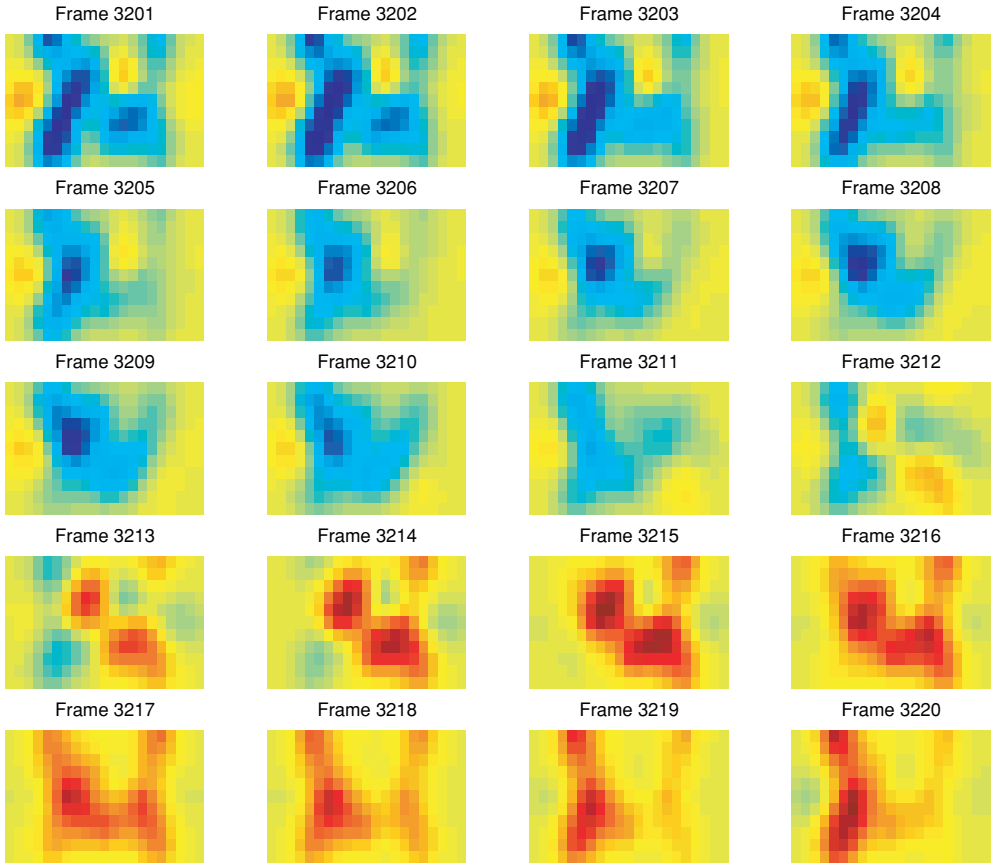


**Figure 5.** Series of 20 reconstructed images from continuous wave data collected by Franceschini *et al* (2000). In each case the scale is the same. The whole series represents a time course of only 0.4 s, and the variation is presumably principally due to arterial pulsation. Note that for the standard reconstruction method, the sampling frequency is eight times lower, and much of the variation seen here would be averaged together. Note that only two measurements were incorporated for the state space estimation at each time instant.

M An MPEG movie of this figure is available from stacks.iop.org/PMB/48/1491.

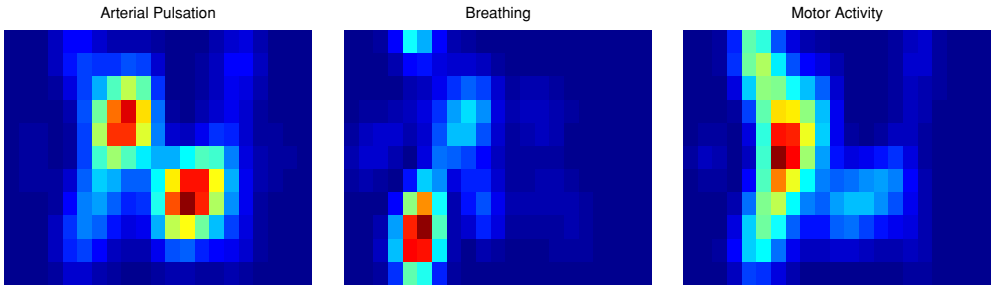


**Figure 6.** Spatial map of activity associated with three temporal components. There is some spatial separation in the activity due to these components. Notably this allows us to isolate the component due to the experimental hand tapping condition which presumably corresponds to the part of the cortex responsible for the motor task.

coming in. Recall that with a static reconstruction we would average eight of these states together. Once more, we have also plotted the mean energy at each frequency in figure 6. The reconstruction allows us to segregate activity that belongs to components at different time scales. The slowest (right-most) component corresponds to changes due to the experimental hand tapping condition and hence represents the part of the cortex which is responsible for the motor task.

## 7. Discussion

Optical measurements have been used to reconstruct the hemodynamics of the human head by Bluestone *et al* (2001), using a technique which considers each (traditional) frame separately. In this paper, we have detailed a general method for the reconstruction of time-series data in optical tomography. Our method is based on a state space formulation in contrast to previous spatio-temporal imaging techniques (Barbour *et al* 1999). The system exploits known patterns in the state of the tissue in order to help solve the difficult ill-posed reconstruction problem. One can view this as implementing 'temporal regularization' for the time-varying reconstruction problem. In this paper we constructed a state update model consisting of a linear sum of three narrow band oscillating components. We then solve for the parameters defining the amplitude and phase of these components. A second advantage of the state space reconstruction is that we can use this model to segment the activity into physiological components which are known to have different time courses and produce dynamic activity maps for each.

A third advantage of the state space reconstruction is that measurements can be incorporated into the system at exactly the time that they were made. To reconstruct each frame of the data separately, we must wait for a full set of source–detector measurements. Since the sources are typically fired alternately, this means that the measurements are spread out in time. The state space reconstruction method permits us to integrate each measurement at the time that it is received as well as ultimately providing a higher temporal resolution to the reconstruction.

## References


Anderson B D O and Moore J B 1979 *Optimal Filtering* (Englewood Cliffs, NJ: Prentice Hall)

Arridge S R 1995 Photon measurement density functions: Part 1. Analytical forms *Appl. Opt.* **34** 7394–409

Arridge S R 1999 Optical tomography in medical imaging *Inverse Problems* **15** 41–93

Arridge S R and Schweiger M 1995 Photon measurement density functions: Part 2. Finite element calculations *Appl. Opt.* **34** 8026–37

Arridge S R, Schweiger M, Hiraoka M and Delpy D T 1993 A finite element approach for modeling photon transport in tissue *Med. Phys.* **20** 299–309

Barbour R L, Graber H L, Schmitz C H, Pei Y and Zhong S 1999 Spatio-temporal imaging of vascular reactivity in optical tomography *Proc. of the Inter-Institute Workshop on in-vivo Optical Imaging at the NIH* pp 161–6

Bluestone A Y, Abdoulaev G, Schmitz C H, Barbour R L and Hielscher A H 2001 Three-dimensional optical tomography of hemodynamics in the human head *Opt. Express* **9** 272–86

Chance B, Zhuang Z, UnAh C and Lipton L 1993 Cognition-activated low-frequency modulation of light absorption in the human brain *Proc. Natl. Acad. Sci.* **90** 3770–4

Chang J, Graber H L, Barbour R L and Aronson R 1996 Recovery of optical cross-section perturbations in dense-scattering media by transport theory based imaging operators and steady state simulated data *Appl. Opt.* **35** 3963–78

Colak S B, Papaiouannou D G, Hooft G W, van der Mark M B, Schomberg H, Paaschens J C J, Mellissen J B M and van Asten N A A J 1997 Tomographic image reconstruction from optical projections in light diffusing media *Appl. Opt.* **36** 180–213

Fantini S, Franceschini M A, Gaida G, Gratton E, Jess H, Mantulin W W, Moesta K T, Schlag P M and Kaschke M 1996 Frequency-domain optical mammography:edge effect corrections *Med. Phys.* **23** 149–57

Franceschini M A, Moesta K T, Fantini S, Gaida G, Gratton E, Jess H, Mantulin W W, Seeber M, Schlag P M and Kaschke M 1997 Frequency domain techniques enhance optical mammography: initial clinical results *Proc. Natl. Acad. Sci. USA* **94** 6468–73

Franceschini M A, Toronov V, Filiaci M E, Gratton E and Fantini S 2000 On-line optical imaging of the human brain with 160-ms temporal resolution *Opt. Express* **6** 49–57

Gaudette R J, Brooks D H, DiMarzio C A, Kilmer M E, Miller E L, Gaudette T and Boas D A 2000 A comparison study of linear reconstruction techniques for diffuse optical tomographic imaging of absorption coefficient *Phys. Med. Biol.* **45** 1051–70

Gratton G, Fabiani M, Corballis P M, Hood D C, Goldman-Wood M R, Hirsch J, Kim K, Friedman D and Gratton E 1997 Fast and localised event-related optical signals (eros) in the human occipital cortex: comparisons with the visual evoked potential and FMRI *Neuroimage* **6** 168–80

Hebden J C, Arridge S R and Delpy D T 1997 Optical imaging in medicine: Part I. Experimental techniques *Phys. Med. Biol.* **42** 825–40

Heino J and Somersalo E 2002 Estimation of optical absorption in anisotropic background *Inverse Problems* **18** 559–73

Kaipio J P, Karjalainen P A, Somersalo E and Vauhkonen M 1999 State estimation in time-varying electrical impedence tomography *Ann. New York Acad. Sci.* **873** 430–9

Kaipio J P and Somersalo E 1999 Nonstationary inverse problems and state estimation *J. Inv. Ill-Posed Problems* **7** 273–82

Kato T, Kamei A, Takashima S and Ozaki T 1993 Human visual cortical function during photic stimulation monitoring by means of near-infrared spectroscopy *J. Cereb. Blood Flow Metab.* **13** 516–20

Kolehmainen V, Prince S, Arridge S R and Kaipio J P 2003 State estimation approach to the non-stationary optical tomography problem *J. Opt. Soc. Am.* A **20** 876–84

Maki A, Yamashita Y, Ito Y, Watanabe E, Mayanagi Y and Koizumi H 1995 Spatial and temporal analysis of human motor activity using non-invasive NIR topography *Med. Phys.* **22** 1997–2005

Maki A, Yamashita Y, Watanabe E and Koizumi H 1996 Visualising human motor activity using non-invasive optical tomography *Frontiers Med. Biol. Eng.* **7** 285–97

Nioka S, Yung Y, Shnall M, Zhao S, Orel S, Xie C, Chance B and Solin L 1997 Optical imaging of breast tumour by means of continuous waves *Adv. Exp. Med. Biol.* **411** 227–32

Paulsen K D and Jiang H 1996 Enhanced frequency-domain optical image reconstruction in tissues through total variation minimization *Appl. Opt.* **35** 3447–58

Rauch H E, Tung F and Striebel C T 1963 Maximum likelihood estimates of linear dynamic systems *AIAA* **3** 1445

Schmitt U and Louis A K 2002 Efficient algorithms for the regularization of dynamic inverse problems: Part 1. Theory *Inverse Problems* **18** 645–58

Schmitt U, Louis A K, Wolters C and Vauhkonen M 2002 Efficient algorithms for the regularization of dynamic inverse problems: Part 2. Applications *Inverse Problems* **18** 659–76

Schweiger M, Arridge S R and Delpy D T 1993 Application of the finite element method for the forward and inverse models in optical tomography *J. Math. Imaging Vis.* **3** 263–83

Schweiger M, Arridge S R, Hiraoka M and Delpy D T 1995 The finite element model for the propagation of light in scattering media: boundary and source conditions *Med. Phys.* **22** 1779–92

Seppänen A, Vauhkonen M, Somersalo E and Kaipio J P 2001b State space models in process tomography—approximation of state noise covariance *Inv. Probl. Eng.* **9** 561–85

Seppänen A, Vauhkonen M, Vauhkonen P J, Somersalo E and Kaipio J P 2001a State estimation with fluid dynamical evolution models in process tomography—an application with impedence tomography *Inverse Problems* **17** 467–84

Tromberg B J, Coquoz O, Fishkin J B, Pham T, Anderson E R, Butler J, Cahn M, Gross J D, Venugopalan V and Pham D 1997 Non-invasive measurements of breast tissue optical properties using frequency-domain photon migration *Phil. Trans. R. Soc.* B **352** 661–8

Vauhkonen M, Karjalainen P A and Kaipio J P 1999 A Kalman filter to track fast impedence changes in electrical impedence tomography *IEEE Trans. Biomed. Eng.* **45** 486–93

Vauhkonen P J, Vauhkonen M and Kaipio J P 2001 Fixed-lag smoothing and state estimation in dynamic electrical impedance tomography *Int. J. Numer. Methods Eng.* **50** 2195–209

Villringer A, Planck J, Hock C, Schleinkofer L and Dirnagl U 1993 Near infrared spectroscopy (NIRS): a new tool to study hemodynamic changes during activation of brain function in human adults *Neurosci. Lett.* **154** 101–4

Walker S A, Fantini S and Gratton E 1997 Image reconstruction by backprojection from frequency domain optical measurements in highly scattering media *Appl. Opt.* **36** 170–9

Wenzel R, Obrig H, Ruben J, Villringer K, Thiel A, Bernardinger J, Dirnagl U and Villringer A 1996 Cerebral blood oxygenation changes induced by visual stimulation in humans *J. Biomed. Opt.* **4** 399–404

Ye J C, Webb K J, Bouman C A and Millane R P 1999 Optical diffusion tomography by iterative coordinate-descent optimization in a Bayesian framework *J. Opt. Soc. Am.* A **16** 2400–12